


Thermal effects on collective modes in disordered s -wave superconductors

Abhisek Samanta,^{1,*} Anirban Das,² Nandini Trivedi ,³ and Rajdeep Sensarma^{4,†}

¹Physics Department, Technion, Haifa 32000, Israel

²School of Physical Sciences, Indian Association for the Cultivation of Science, Jadavpur, Kolkata 700032, India

³Department of Physics, The Ohio State University, Columbus, Ohio 43201, USA

⁴Department of Theoretical Physics, Tata Institute of Fundamental Research, Mumbai 400005, India



(Received 9 April 2021; revised 30 September 2021; accepted 24 February 2022; published 4 March 2022)

We investigate the effect of thermal fluctuations on the two-particle spectral function for a disordered s -wave superconductor in two dimensions, focusing on the evolution of the collective amplitude and phase modes. We find three main effects of thermal fluctuations: (1) the phase mode is softened with increasing temperature, reflecting the decrease of superfluid stiffness; (2) remarkably, the nondispersive collective amplitude modes at finite energy near $\mathbf{q} = [0, 0]$ and $\mathbf{q} = [\pi, \pi]$ survive even in the presence of thermal fluctuations in the disordered superconductor; and (3) the scattering of the thermally excited fermionic quasiparticles leads to low-energy incoherent spectral weight that forms a strongly momentum-dependent background halo around the phase and amplitude collective modes and broadens them. Due to momentum and energy conservation constraints, this halo has a boundary which disperses linearly at low momenta and shows a strong dip near the $[\pi, \pi]$ point in the Brillouin zone.

DOI: [10.1103/PhysRevB.105.104503](https://doi.org/10.1103/PhysRevB.105.104503)

I. INTRODUCTION

The quantum phase transition between superconducting and insulating phases of two-dimensional films, driven by increasing disorder [1–6], provides a paradigm for the complex interplay of interaction and localization [7–11]. The single-particle fermionic spectrum remains gapped throughout the transition [9,12] and the fluctuations of the local superconducting order parameter, that describe the phase (Goldstone) and amplitude (Anderson-Higgs) collective modes, are the key low-energy excitations that drive this phase transition [13–15].

The Higgs mode in superconductors has a long history [16–18] and continues to be a topic of tremendous current interest [15,19–30]. While the observation of the Higgs particle in particle colliders [31,32] has been hailed as one of the recent successes in that field, the corresponding mode has not been observed in a clean superconductor. This is due to the fact that in a clean superconductor, this mode sits at the two-particle continuum threshold and is damped [17]. Early predictions [33] that the mode can be seen as a subgap feature in systems with accompanying charge density order has recently been experimentally verified [34]. The area has also received a lot of attention due to clean observation of the Higgs mode in a charge neutral ultracold atomic system [13] near the superfluid-insulator transition. Recently, observation of low-energy optical spectral weight in disordered superconductors [14] close to a disorder-driven superfluid-insulator transition has led to a conjecture that this weight is due to the Higgs mode, based on earlier work on optical conductivity in

clean systems [35,36]. More recent theoretical work [37,38] has looked at the question of the contribution of collective modes to optical conductivity in disordered superconductors at zero temperature.

In an earlier work [39], we studied the evolution of two-particle pair spectral functions [39–43] in a disordered superconductor and presented their full momentum and frequency dependence as a function of disorder at zero temperature. We found the expected (a) continuum of two-particle excitations, above an energy threshold equal to twice the single-particle gap, and (b) linearly dispersing low-energy collective modes. In addition, surprisingly, we found additional spectral weight at finite energies below the two-particle continuum in the long-wavelength limit. The weight in this nondispersive feature, which was spectrally separated from the linearly dispersing collective modes, increased with increasing disorder strength. We were able to correlate this nondispersive spectral weight with the Higgs mode and the low-energy Higgs weight was concentrated in this additional spectral feature in the two-particle pair spectral function. One obvious question is, How does that picture change in the presence of temperature? It is crucial to understand the combined role of both thermal and quantum fluctuations to make connections with experimental data.

We also found that at arbitrarily weak disorder, the zero momentum Anderson-Higgs mode that sits at the threshold of the two-particle continuum, shifts *nonperturbatively* within the two-particle gap. This subgap feature of the Anderson-Higgs mode is distinguishable from the low-energy phase divergence at all disorder values, making it a possible candidate to observe in energy-resolved spectroscopies. Therefore, the natural question that arises is, What is the fate of the Anderson-Higgs mode as a function of temperature? Is it still possible to separate this mode from the phase fluctuations at

*abhiseks@campus.technion.ac.il

†sensarma@theory.tifr.res.in

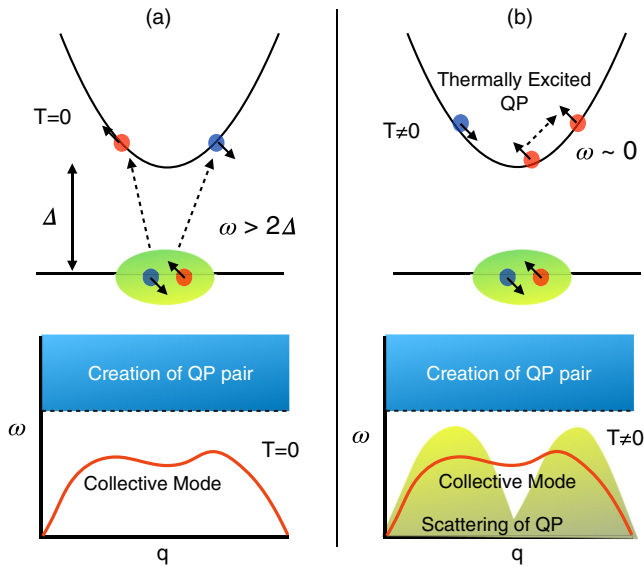


FIG. 1. (a) At $T = 0$, the breaking of the Cooper pair into two quasiparticles leads to a two-particle continuum in the pair spectral weight with a threshold of 2Δ . The lower part of the figure depicts a schematic of the features of the pair spectral function at $T = 0$. (b) At finite temperature, the scattering of thermally excited quasiparticles leads to additional low energy incoherent spectral weight. This leads to a halo behind the collective modes, as shown in the lower part of the figure.

finite temperatures? We address these important questions in this paper.

Our theoretical approach involving functional integrals allows us to investigate the different contributions of the amplitude, the phase, and amplitude-phase mixing fluctuations to the two-particle spectral function at finite temperature. The key features of our analysis are the following: (i) We obtain the evolution of the Anderson-Higgs and the Goldstone mode as a function of both temperature and disorder. (ii) We find that small thermal fluctuations induce additional low-energy incoherent spectral weight that forms lobes below the two-particle gap, which compete with the collective mode structure in the amplitude sector, but keep the phase sector mostly unaffected. (iii) In the presence of weak disorder, the subgap Anderson-Higgs mode can be observed separately from the low-energy phase pile-up in an energy-resolved way even in presence of moderately high temperatures, thereby making it a robust feature of disordered superconductors. We note that an alternative approach based on an effective classical Monte Carlo has been used to treat disordered superconductors at finite temperature [44] but it does not provide momentum-resolved information about the amplitude and phase fluctuations.

The two-particle continuum at $T = 0$ is formed microscopically by breaking up a Cooper pair into a pair of single-particle excitations, as shown in Fig. 1(a), and requires a threshold energy of twice the single-particle gap. On the other hand, the collective mode is better described in terms of the long-wavelength fluctuations of the amplitude and phase of the condensate of the Cooper-pairs (i.e., the order parameter). As temperature is raised, changes in the pair spectral function occur by two processes: (1) The collective mode

dispersion flattens as the superfluid stiffness is reduced at finite temperatures due to thermally excited quasiparticles and (2), additionally, another incoherent continuum is formed due to scattering of these thermally populated quasiparticles, as shown in Fig. 1(b). This leads to a low-energy diffuse background weight and consequent broadening of the collective modes. In a clean system, the incoherent thermal excitations occur only below an upper energy cutoff $\epsilon_{\text{cutoff}}(q)$ determined by energy and momentum conservation in the scattering process. $\epsilon_{\text{cutoff}}(q)$ varies linearly at long wavelengths and shows a prominent dip around the commensurate wave vector $[\pi, \pi]$.

In a weakly disordered system, the behavior of the energy cutoff and its momentum dependence continues to hold with small corrections. As a result, the nondispersive spectral weight observed at finite subgap energy at long wavelengths remains sharp at finite temperatures for weakly disordered systems. For strongly disordered systems, the constraint due to momentum conservation in a scattering process is no longer applicable, and we find the incoherent spectral weight as a diffused halo without sharply defined boundaries. Since the low-energy weight in the diffuse halo comes from the scattering of thermally excited quasiparticles, it is exponentially suppressed at low temperatures and significant weight develops only when a fraction of the critical temperature T_c is approached.

In disordered systems, the presence of a reasonably sharp threshold of the incoherent weight at long wavelengths leads to a clear visibility of the long-wavelength finite energy weight in the Higgs spectrum. This spectral feature, which was seen clearly in the $T = 0$ calculations [39], thus survives thermal fluctuations in the system. This is a key insight that we obtain from these calculations.

The rest of the paper is organized as follows: In Sec. II, we discuss the model Hamiltonian for disordered superconductors and the finite-temperature mean-field theory. In Sec. III, we first discuss the technical details of the finite-temperature Gaussian fluctuation calculation before turning our attention to the pair spectral function in clean systems at finite temperature in Sec. III A. In Sec. III B, we focus on the finite-temperature evolution of the pair spectral function in the disordered system. Finally, we conclude with a brief overview of our calculation and key results.

II. MEAN-FIELD THEORY AT FINITE TEMPERATURES

We study the attractive Hubbard model on a square lattice in the presence of on-site nonmagnetic impurities. The Hamiltonian for the model is given by

$$H = -t \sum_{\langle rr' \rangle \sigma} (c_{r\sigma}^\dagger c_{r'\sigma} + h.c.) - U \sum_r n_{r\uparrow} n_{r\downarrow} + \sum_r (v_r - \mu) n_r, \quad (1)$$

where $c_{r\sigma}^\dagger$ ($c_{r\sigma}$) is the creation (annihilation) operator for an electron with spin σ on site r and μ is the chemical potential. Nearest-neighbor hopping between two electrons is governed by t , and U is the attractive interaction between two electrons on the same site which leads to Cooper pairing. Here, v_r is an on-site random potential, which is drawn independently on every site r from a uniform distribution of zero mean and width V , i.e., $v_r \in [-V/2, V/2]$. Therefore, V corresponds

to the strength of the disorder. This model has been studied previously [9] at zero temperature within a spatially inhomogeneous Bogoliubov–de Gennes (BdG) mean-field theory. More recently, the two-particle spectral functions in this model at $T = 0$ have been studied within a Gaussian expansion around the BdG solution [39]. In this section, we investigate the mean-field theory at finite temperatures, while later sections will be devoted to considering the fluctuations around the mean-field theory at finite temperatures.

Within a functional integral formalism, the partition function for the model is given by

$$Z = \int D[\bar{f}_\sigma, f_\sigma] e^{-S[\bar{f}_\sigma, f_\sigma]}. \quad (2)$$

Here the imaginary time (τ) action S in terms of the fermion fields $[\bar{f}_\sigma(r, \tau), f_\sigma(r, \tau)]$ is given by

$$S = \int_0^\beta d\tau \sum_{rr', \sigma} \bar{f}_\sigma(r, \tau) [\partial_\tau \delta_{rr'} + H_{rr'}^0] f_\sigma(r', \tau) - U \sum_r \bar{f}_\uparrow(r, \tau) \bar{f}_\downarrow(r, \tau) f_\downarrow(r, \tau) f_\uparrow(r, \tau), \quad (3)$$

where $\beta = 1/T$ and the single-particle Hamiltonian $H_{rr'}^0 = -t\delta_{(rr')} - (\mu - v_r)\delta_{rr'}$. We introduce two Hubbard-Stratonovich auxiliary fields, $\Delta(r, \tau)$ that couples to the particle-particle channel $[\bar{f}_\uparrow(r, \tau)\bar{f}_\downarrow(r, \tau)]$ and the field $\xi(r, \tau)$ that couples to the density channel $[\bar{f}(r, \tau)f(r, \tau)]$ to construct a quadratic theory in the fermion fields. Integrating out the fermions, and considering a static but spatially varying saddle point profile of the auxiliary fields, $\Delta(r, \tau) = \Delta_0(r)$ and $\xi(r, \tau) = \xi_0(r)$, lead to the BdG mean-field theory. The BdG self-consistency equations at finite T are given by

$$\Delta_0(r) = U \sum_n u_n(r) v_n^*(r) (1 - 2F_n(T)), \quad (4)$$

$$\xi_0(r) = U \sum_n (1 - 2F_n(T)) |v_n(r)|^2 + F_n(T) |u_n(r)|^2, \quad (5)$$

$$\text{and } \langle n \rangle = \frac{2}{N_s} \sum_r \frac{\xi_0(r)}{U}, \quad (6)$$

where $\langle n \rangle$ is the average density of electrons in the system with N_s number of sites. Here $[u_n(r), v_n(r)]$ are the eigenvectors of the BdG matrix corresponding to eigenvalue E_n and n runs over positive eigenvalues ($E_n > 0$) only. The Fermi function at temperature T is given by $F_n(T) = \frac{1}{e^{E_n/T} + 1}$. We solve the BdG self-consistency equations [Eqs. (4)–(6)] on a 24×24 square lattice with an interaction strength $U/t = 5$ and at an average fermion density $\langle n \rangle = 0.875$. We consider 15 disorder realizations for each disorder.

Before we discuss the results of the mean-field theory at finite temperatures, we note the main features of the mean-field theory at zero temperature for disordered superconductors [9,39]: (i) The distribution of the local pairing amplitude evolves from a sharp distribution around an average value for low disorder to a broad distribution with peaks around zero for large disorder, which indicates the destruction of superconductivity. (ii) The distribution of local densities evolves from a sharp unimodal distribution at low disorder to a broad bimodal distribution at large disorder. This indicates the formation of superconducting puddles or patches in the

background of nonsuperconducting regions at large disorder. (iii) The formation of superconducting patches is further confirmed by the spatial distribution of the pairing amplitude that shows cluster formation on the scale of the coherence length in typical disorder configurations. (iv) The single-particle gap remains finite and large at strong disorder, while the average order parameter and the superfluid density both decrease monotonically at large disorder. We will next compare and contrast these features to the behavior at finite temperatures.

Temperature dependence of single-particle gap: Figure 2(a) shows the single-particle gap in the system as a function of temperature. The gap for a clean superconductor ($V = 0$) vanishes around $T_c = 1.1 t$. Note that while the $T = 0$ gap has reduced by a factor of 2 between the clean case and $V = 3 t$, the decrease in the mean-field T_c is much smaller. A similar trend is seen in Fig. 2(b) where we plot the average pairing amplitude Δ_{OP} (averaged over sites and over disorder realizations) as a function of temperature for different values of disorder. Once again we note that while $\Delta_{OP}(T = 0)$ reduces by a factor of four as we go from $V = 0$ to $V = 3 t$, T_c only changes from $1.1 t$ to $0.9 t$. These two trends taken together show that within the mean-field theory disorder is much more effective at reducing/killing superconductivity at $T = 0$ compared to its effect on reducing T_c of the system.

A. Temperature dependence of superfluid stiffness

A similar trend is seen in the temperature variation of the superfluid stiffness ρ_s (see Appendix A), which is plotted in Fig. 2(c) with increasing disorder. While the $T = 0$ value of ρ_s reduces by a factor of 6 as the disorder is ramped up from the clean case to $V = 3 t$, the mean-field transition temperature T_c only changes from $1.1 t$ to $0.9 t$.

We note that in two dimensions, the finite temperature transition is in the universality class of the Berezinskii-Kosterlitz-Thouless (BKT) transition controlled by phase fluctuations. We obtain an estimate of T_{BKT} from the intersection of the line $y = \frac{2}{\pi} T$ with $\rho_s(T)$ obtained from our calculations, $\rho_s(T_{\text{BKT}}^-) = \frac{2}{\pi} T_{\text{BKT}}$ [see Fig. 2(c)]. We see that with increasing disorder, the mean field T_c is largely unaffected by disorder. However, the zero temperature superfluid stiffness is reduced by a factor of 6 as disorder is increased to $V = 6t$, resulting in a strong reduction of the BKT transition temperature.

B. Distributions

It is useful to look at how the distribution of the local order parameter $\Delta(r)$ and the local density $n(r)$ changes with temperature and disorder strength. In Figs. 3(a) and 3(b), we plot the distribution of $\Delta(r)$ for $V = 0.1 t$ and $V = t$, respectively. Each plot shows the distribution for a range of temperatures. In each of these cases, we see that the shape of the distribution does not change much with temperature, although the distribution shifts to lower values of Δ , consistent with the decrease of Δ with temperature. In Fig. 3(c), we see a similar trend with a pileup around $\Delta = 0$. Note that for $V = t$ and $V = 3 t$, $T = t$ is above T_c and we simply get all the weight at $\Delta = 0$. We plot the distribution of local densities for

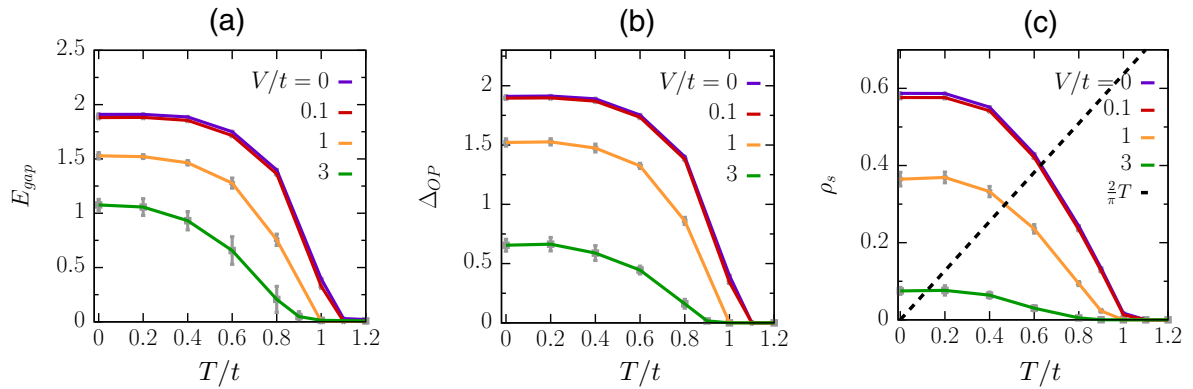


FIG. 2. (a) Single-particle excitation gap E_{gap} , (b) superconducting order parameter Δ_{OP} , and (c) superfluid stiffness ρ_s as a function of temperature T , obtained from finite T BdG calculation. We present data for clean system ($V = 0$) and three disorder values, $V = 0.1 t$, t and $3 t$. E_{gap} and Δ_{OP} vanish at $T_c = 1.1 t$ in the clean system. All three parameters, E_{gap} , Δ_{OP} , and ρ_s have reduced significantly at $T = 0$, while the decrease in mean-field T_c is much smaller. The data have been obtained on a 24×24 square lattice and averaged over 15 disorder realizations. In (c), we also show $y = \frac{2}{\pi} T$ (dashed line) whose intersection with $\rho_s(T)$ gives an estimate of the BKT transition temperature.

$V = 0.1 t$, $V = t$, and $V = 3 t$ in Figs. 3(d)–3(f) respectively. The density distribution goes from a unimodal distribution at low disorder to a bimodal distribution at high disorder. At all values of disorder, the distribution narrows with increasing temperature, with the effect clearly visible at large disorder strengths. At large disorder, the bimodal distribution comes from the formation of superconducting and nonsuperconducting patches. Increasing temperature leads to smoother density

profile between the patches and hence to a narrowing of the density distributions.

III. GAUSSIAN FLUCTUATIONS AND PAIR SPECTRAL FUNCTIONS

The primary motivation of this paper is to understand how the fluctuations around the mean-field theory that dominate

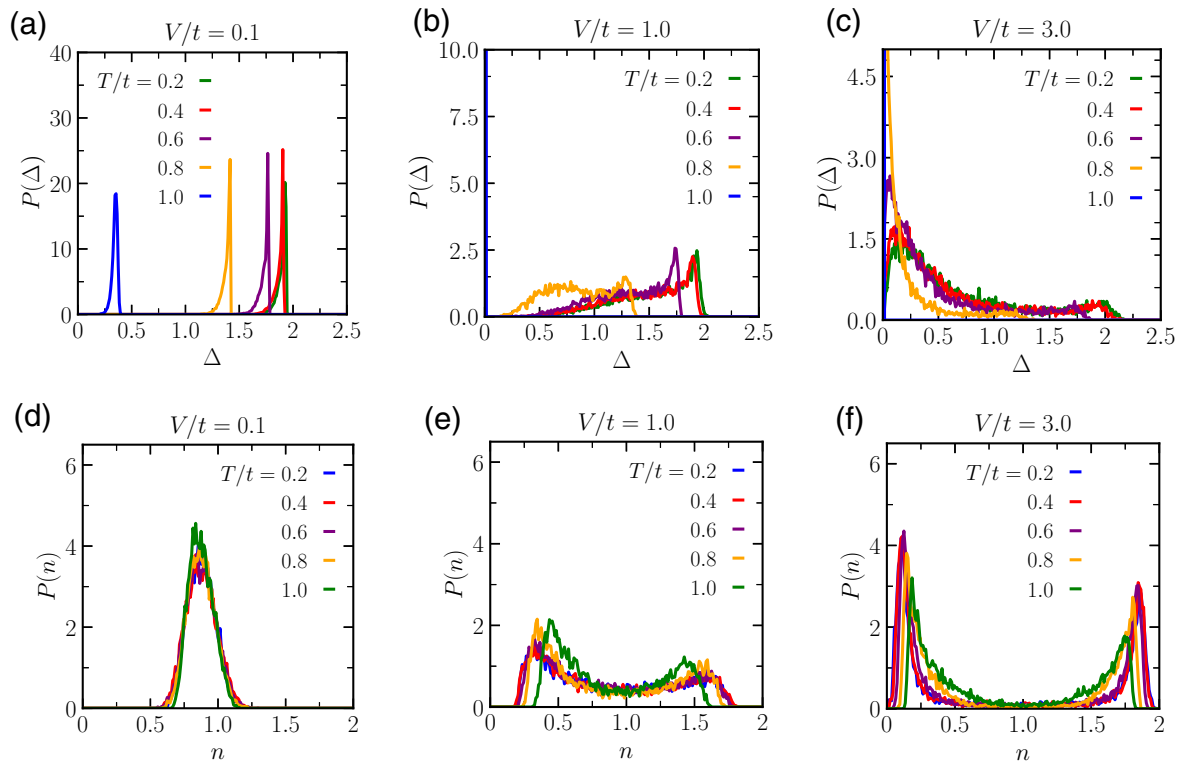


FIG. 3. Distribution of (a)–(c) local superconducting pairing amplitude $\Delta(r)$ and (d)–(f) local density $n(r)$ obtained from finite T BdG calculation for different values of disorder V and temperature T . With increasing disorder, $P(\Delta)$ changes from a sharp distribution around the average Δ to a broad distribution with peaks around 0. For a fixed V , the shape of $P(\Delta)$ does not change much with temperature, while the distribution shifts toward the lower value of Δ . On the other hand, $P(n)$ becomes bimodal around the average density $\langle n \rangle = 0.875$ in the presence of strong disorder, and with increasing the temperature, the distribution becomes narrower.

the two-particle pair spectral function at low energies evolve with temperature in a disordered superconductor. To this end, we include the spatiotemporal fluctuations of the Δ field through

$$\Delta(r, \tau) = (\Delta_0(r) + \eta(r, \tau))e^{i\theta(r, \tau)}, \quad (7)$$

where $\eta(r, \tau)$ and $\theta(r, \tau)$ are the amplitude and the phase fluctuations, respectively, around the BdG saddle point solution $\Delta_0(r)$. We expand the action to second order in the fluctuations to obtain the Gaussian action S_G corresponding to the fluctuations of the order parameter at finite temperature T (for $T = 0$, see Ref. [39]),

$$S_G = \sum_{r,r'} \sum_{\omega_m} (\eta(r, \omega_m) \quad \theta(r, \omega_m)) \begin{pmatrix} D^{-1}_{11}(r, r', \omega_m) & D^{-1}_{12}(r, r', \omega_m) \\ D^{-1}_{21}(r, r', \omega_m) & D^{-1}_{22}(r, r', \omega_m) \end{pmatrix} \begin{pmatrix} \eta(r', -\omega_m) \\ \theta(r', -\omega_m) \end{pmatrix}, \quad (8)$$

where $\omega_m = (2m)\pi/\beta$ is the bosonic Matsubara frequency. We analytically continue from Matsubara to real frequencies to construct the real-time inverse fluctuation propagators. We note that our formalism does not suffer from issues of numerical analytic continuation.

The inverse fluctuation propagator corresponding to the amplitude fluctuation, D^{-1}_{11} , is given by

$$D^{-1}_{11}(r, r', \omega) = \frac{1}{U} \delta_{rr'} + \frac{1}{2} \sum_{E_n, E_{n'} > 0} f_{nn'}^{(1)}(r) f_{nn'}^{(1)}(r') \chi_{nn'}(\omega) + \frac{1}{2} \sum_{E_n, E_{n'} > 0} f_{nn'}^{(2)}(r) f_{nn'}^{(2)}(r') \zeta_{nn'}(\omega), \quad (9)$$

where

$$f_{nn'}^1(r) = [u_n(r)u_{n'}(r) - v_n(r)v_{n'}(r)], \quad \text{and} \quad f_{nn'}^2(r) = [u_n(r)v_{n'}(r) + v_n(r)u_{n'}(r)] \quad (10)$$

are the matrix elements related to the BdG wave functions and the temperature-dependent functions χ and ζ are given by

$$\begin{aligned} \chi_{nn'}(\omega) &= \left(\frac{1}{\omega + i0^+ - E_n - E_{n'}} - \frac{1}{\omega + i0^+ + E_n + E_{n'}} \right) (1 - F_n(T) - F_{n'}(T)) \quad \text{and} \\ \zeta_{nn'}(\omega) &= \left(\frac{1}{\omega + i0^+ + E_n - E_{n'}} - \frac{1}{\omega + i0^+ - E_n + E_{n'}} \right) (F_n(T) - F_{n'}(T)). \end{aligned} \quad (11)$$

It is useful to analyze the structure of χ and ζ , since they occur in all the matrix elements of the inverse fluctuation propagators and provide insight about the microscopic processes that control the temperature dependence of the pair spectral function. Here ζ represents (up to matrix elements, which do not change its singularity structure) the probability amplitude of scattering a Bogoliubov quasiparticle from one state to the other. Note that $F_n(T) = 0$ for all gapped states at $T = 0$ and hence this term does not contribute to the collective modes around the ground state. A simple way to understand this is that the quasiparticles need to be present in the first place to be scattered, and at $T = 0$, none of the gapped modes are excited in the system. As temperature is raised, this amplitude becomes finite. It is important to note that the singularities of this function occur when $\omega = E_n - E_{n'}$, and hence at very low energies. Thus, at finite temperatures, ζ is complex at low energies, with an amplitude that increases with temperature. We will later see that these scattering processes play a very important role in determining the low-energy pair spectral function at finite temperatures. We now consider the structure of χ , which represents (up to matrix elements, which do not change the singularity structure of these functions) the amplitude for creating a pair of Bogoliubov quasiparticles. This is reflected in the singularities at $\omega = \pm(E_n + E_{n'})$. Hence, for $\omega < 2E_{\text{gap}}$, where the fermionic single-particle gap E_{gap} corresponds to the lowest positive eigenvalue of the BdG Hamiltonian, χ is purely real, while it takes complex values for $\omega > 2E_{\text{gap}}$. If we consider the numerator of χ , it is evident that the numerator goes to 1 at $T = 0$. So, the $T = 0$ spectral function is completely dominated by this term. As the temper-

ature is raised, the numerator decreases; however, χ remains real at low energies below the two-particle continuum as long as the single-particle gap remains finite.

The inverse fluctuation propagator for the phase fluctuation D^{-1}_{22} is given by

$$D^{-1}_{22}(r, r', \omega) = \tilde{D}_{\text{dia}}(r, r') + \omega^2 \kappa(r, r', \omega) + \Lambda(r, r', \omega), \quad (12)$$

where \tilde{D}_{dia} is the diamagnetic response of the system, κ is the frequency dependent compressibility and $\Lambda(r, r', \omega)$ is related to the paramagnetic current-current correlator on the lattice. The exact formulas for \tilde{D}_{dia} , κ , and Λ are given in Appendix B.

Finally, the inverse fluctuation propagator corresponding to amplitude-phase mixing, D^{-1}_{12} , is given by

$$\begin{aligned} D^{-1}_{12}(r, r', \omega) &= -\frac{i\omega}{4} \sum_{E_n, E_{n'} > 0} f_{nn'}^{(1)}(r) f_{nn'}^{(2)}(r') \chi_{nn'}(\omega) \\ &\quad + f_{nn'}^{(1)}(r') f_{nn'}^{(2)}(r) \zeta_{nn'}(\omega). \end{aligned} \quad (13)$$

We invert the matrix $D_{\alpha\beta}^{-1}(r, r', \omega)$ to obtain the fluctuation propagators $D_{\alpha\beta}(r, r', \omega)$ and the corresponding spectral functions, $\mathcal{P}_{\alpha\beta}(r, r', \omega) = -\frac{1}{\pi} \text{Im} D_{\alpha\beta}(r, r', \omega)$. Here $\mathcal{P}_{11}(r, r', \omega) = -\frac{1}{\pi} \text{Im}(\eta(r, \omega + i0^+) \eta(r', -\omega + i0^+))$ corresponds to amplitude or Higgs fluctuations, $\mathcal{P}_{22}(r, r', \omega) = -\frac{1}{\pi} \text{Im}(\theta(r, \omega + i0^+) \theta(r', -\omega + i0^+))$ denotes the phase fluctuations while the amplitude-phase mixing is governed by $\mathcal{P}_{12}(r, r', \omega) = -\frac{1}{\pi} \text{Im}(\eta(r, \omega + i0^+) \theta(r', -\omega + i0^+))$. However, the phase fluctuation propagators are not directly

measurable in experiments, where probes couple to the electron density or current. As shown in Ref. [39], the experimentally measurable pair spectral function

$$P(r, r', \omega) = \sum_{\alpha\beta} P_{\alpha\beta}(r, r', \omega), \quad (14)$$

where $P_{11} = \mathcal{P}_{11}$, $P_{12}(r, r', \omega) = \Delta_0(r)\mathcal{P}_{12}(r, r', \omega)$, $P_{21}(r, r', \omega) = \Delta_0(r')\mathcal{P}_{21}(r, r', \omega)$, and $P_{22}(r, r', \omega) = \Delta_0(r)\Delta_0(r')\mathcal{P}_{22}(r, r', \omega)$.

Note that in a translation invariant system, P and \mathcal{P} are related by simple scaling factors. However, in a disordered system, where the pairing amplitude $\Delta_0(r)$ is varying in space, the spatial correlations of \mathcal{P} and P will be quite different and hence it is important to study the physically measurable correlations.

A. Pair spectral function in a clean superconductor

In this paper, we are primarily interested in studying the temperature dependence of the collective modes and the resultant two-particle spectral functions for a disordered superconductor. We start with the behavior of the temperature dependence of the two-particle spectral function $P(q, \omega)$ in the clean limit ($V/t = 0$). This allows us to interpret the low-energy spectral functions in terms of a temperature-broadened collective mode and a background spectral weight arising from the scattering of thermally excited quasiparticles. This framework will then be used to investigate the pair of spectral functions in the disordered case.

For a clean system, the problem simplifies considerably since the fluctuation propagators are diagonal in the momentum basis; e.g.,

$$D^{-1}_{11}(q, \omega) = \frac{1}{U} + \frac{1}{2} \sum_k [f_k^{(1)}(q)]^2 \chi_k(q, \omega) + [f_k^{(2)}(q)]^2 \zeta_k(q, \omega), \quad (15)$$

where

$$f_k^{(1)}(q) = u_k u_{k+q} - v_k v_{k+q}, \quad f_k^{(2)}(q) = u_k v_{k'} + v_k u_{k'}, \quad (16)$$

with

$$\chi_k(q, \omega) = \left(\frac{1}{(\omega + i0^+ - E_k - E_{k'})} - \frac{1}{(\omega + i0^+ + E_k + E_{k'})} \right) \times [1 - F_k(T) - F_{k'}(T)], \quad (17)$$

$$\zeta_k(q, \omega) = \left(\frac{1}{(\omega + i0^+ + E_k - E_{k'})} - \frac{1}{(\omega + i0^+ - E_k + E_{k'})} \right) \times [F_k(T) - F_{k'}(T)]. \quad (18)$$

In the above formulas, we have used the standard BCS spectrum $E_k = \sqrt{\xi_k^2 + \Delta_0^2}$ with $\xi_k = -2t(\cos k_x + \cos k_y) - \mu$, Δ_0 the uniform pairing amplitude and $u_k^2 = 1/2(1 + \xi_k/E_k) = 1 - v_k^2$.

Figures 4(a)–4(d) show the amplitude spectral function $P_{11}(q, \omega)$, while Figs. 4(e)–4(h) show the phase spectral function $P_{22}(q, \omega)$ in the clean system with increasing temperature. Here the attractive interaction $U = 5t$ and the density is set to 0.875. Let us first focus on the pair spectral functions

at $T = 0$ [Figs. 4(a) and 4(e)]. There is diffuse continuum spectral weight above $\omega > 2\Delta_0$, corresponding to propagation of two Bogoliubov quasiparticles. Note that at $T = 0$, the ζ terms do not contribute, while χ is complex only for $\omega > 2\Delta_0$. For $\omega < 2\Delta_0$, there is a coherent dispersing peak at the collective mode frequencies determined by the vanishing of the determinant of the inverse fluctuation propagator. The mode disperses linearly at low momenta.

At $q = 0$, the collective mode is a pure phase Goldstone mode and the weight of the amplitude component goes to 0. This is clearly shown in the inset of Fig. 4(a), where we plot the weight of amplitude spectral function P_{11} at the collective mode frequency as a function of q . Thus at $q = 0$, the Higgs weight is finite only at $2\Delta_0$, which is well-known [33,45,46]. Furthermore, the Higgs mode at this threshold energy is not a well-defined mode as it is damped due to the presence of the two-particle continuum, hence its weight appears as part of the diffuse continuum (see Appendix C for details). At finite q , however, the collective mode is a mixture of amplitude and phase fluctuations at finite momenta [45], i.e., the eigenmode at finite q has finite projections in both the amplitude and phase sectors. As the temperature is raised to $T = 0.18 T_c$ [Fig. 4(b)], $T = 0.36 T_c$ [Fig. 4(c)], and $T = 0.54 T_c$ [Fig. 4(d)], a thermally broadened collective mode is clearly present riding on a distinct background halo.

The Higgs spectral function P_{11} shows incoherent spectral weight beyond the two-particle continuum $\omega > 2\Delta_0$, corresponding to overdamped modes. This can be contrasted with the nonlinear response of the superconductor to an electromagnetic perturbation or the Higgs contribution to the third-harmonic generation (THG) intensity [15,28,30], which shows a sharp feature at $\omega = 2\Delta_0$. Note that the nonlinear response corresponds to a different correlation function than the spectral function (which represents a linear response of the system) studied here [37–39].

We now discuss the amplitude-phase mixing in our analysis. We note that specially fine-tuned points having additional particle-hole symmetry (e.g., square lattice with only nearest neighbor hopping at exactly half filling) leads to vanishing of amplitude-phase mixing [37]; however, our system does not have this symmetry (average density $\langle n \rangle = 0.875$, away from half filling) and the amplitude-phase mixing is finite at any finite q in the translation invariant system.

Next we study the finite temperature properties of the amplitude and phase spectral functions. The background halo in the spectral function at finite temperatures, which is due to the scattering of the quasiparticles already present in the system (the ζ terms), increases in intensity with increasing temperature. This incoherent spectral weight has some interesting characteristics. At each q , there is an upper bound of energy beyond where there is no incoherent spectral weight, till one reaches $\omega = 2\Delta_0$. This limiting energy, which is the maximum of $|E_k - E_{k+q}|$ for a fixed q , disperses linearly at small q and shows a sharp dip around the Γ and M ($[\pi, \pi]$) points. In Fig. 5(a), we plot the dispersion of the quasiparticle energy E_k as a function of k in the Brillouin zone. We see that the wave vector $q = [\pi, \pi]$ only connects points in the Brillouin zone where the values of E_k do not differ much, leading to a dip in the temperature-dependent background halo around the M point. Although only one such connection

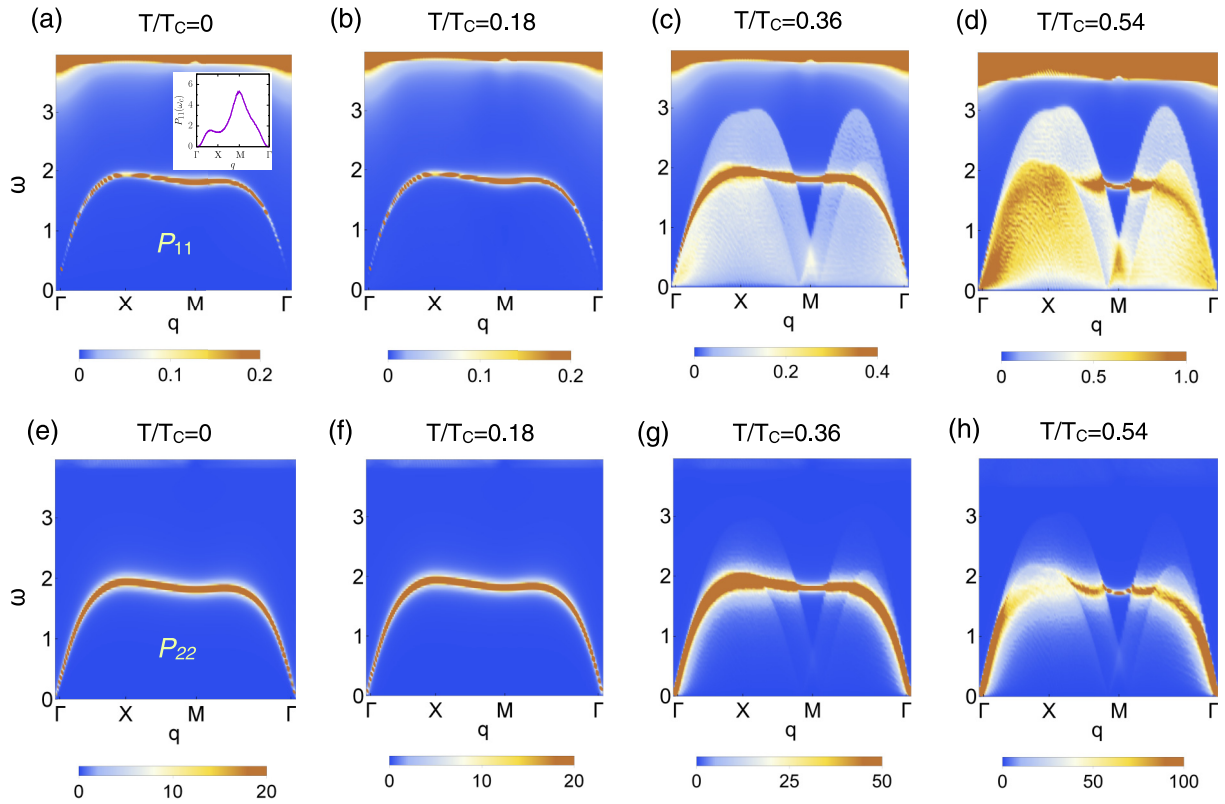


FIG. 4. Spectral functions in clean superconductor: (a)–(d) amplitude spectral function P_{11} and (e)–(h) phase spectral function P_{22} of the pair spectral function $P(q, \omega)$ in a clean superconductor ($V/t = 0$) shown as a density plot in q (along the principle axis of the 2D Brillouin zone of the square lattice) and ω for increasing temperatures: $T = 0$, $T = 0.18 T_c$, $T = 0.36 T_c$, and $T = 0.54 T_c$ (corresponding to $T = 0$, $T = 0.2 t$, $T = 0.4 t$, and $T = 0.6 t$, respectively). At small temperatures, both the spectral functions P_{11} and P_{22} consist of the collective modes below two-particle continuum. The inset of (a) shows P_{11} at the collective mode frequency $[\omega_c(q)]$ at $T = 0$, as a function of q . It clearly shows that the amplitude component of the low-energy dispersive collective mode vanishes as $q \rightarrow 0$. Hence in the clean superconductor at $q = 0$, the Higgs weight is finite only at $2\Delta_0$ (indicated by the large spectral weight at the top edge of (a)–(d)) in the long-wavelength limit. The temperature-dependent background halo is clearly seen in P_{11} for $T = 0.36 T_c$ and $T = 0.54 T_c$, while P_{22} is mostly dominated by strong collective modes. All data for the clean superconductors have been obtained on a 100×100 square lattice.

is shown in the figure, one can easily see that this is true in general. The same also holds for the Γ point. On the contrary, the wave vector $q = [\pi, 0]$ can connect points in the Brillouin zone where the values of E_k can vary from a small to large value, and hence the lobelike structure extends up to a large value of ω . As a result, one can see that the collective mode both at $q = 0$ and $q = [\pi, \pi]$ remain sharp, while there is considerable broadening at intermediate momenta. This is clearly seen in Figs. 4(c) and 4(d), where the apparent width of the collective mode shrinks near the M point when the collective mode lies above the band of incoherent spectral weight. This is also shown in Fig. 5(b), where we plot the line cuts of the Higgs spectral function along the energy axis [energy distribution curve (EDC)] for fixed values of momenta at the largest temperature $T = 0.54 T_c$. Near the zone center, the spectral weight lies above the two-particle continuum. As we move along the q_x axis, the modes at $[\pi/2, 0]$ and $[\pi, 0]$ do not show up as sharp peaks due to the large background incoherent weight. However, at $[\pi, \pi]$, one can clearly see two bumps in the spectral function, the lower one coming from the incoherent scattering of quasiparticles and the upper one corresponding to the coherent collective mode in the system.

We note that the background halo is more clearly seen in the Higgs spectral functions, while the phase spectral functions [Figs. 4(e)–4(h)] are primarily dominated by the large collective mode peak. The robust linear dispersion of the phase mode allows us to extract the speed of sound from the long-wavelength linear dispersion. This speed of sound c_s is plotted as a function of T/T_c in Fig. 5(e). We see that at low temperatures c_s remains almost constant, whereas near $T/T_c \sim 0.54$ it starts decreasing and drops to zero at T_c . The background spectral weight in the phase sector is clearly seen only around $T = 0.54 T_c$ [Fig. 4(h)], where the characteristics are similar to that of the Higgs spectral weight. The EDC curves for the phase spectral function at fixed momenta are plotted in Fig. 5(c). Here it is clear that the coherent spectral weight in the collective mode is much larger than the incoherent spectral weight. Hence, near the collective mode frequency, one can expand the phase spectral function $P_{22}(q, \omega) \sim Z(q)/(\omega - \omega(q) + i\sigma_\omega(q))$. The large coherent spectral weight in the phase channel allows us to extract an energy width of the peak, σ_ω , from the line cuts in Fig. 5(c). This width is plotted as a function of momenta for different temperatures in Fig. 5(d). It is clear that the collective

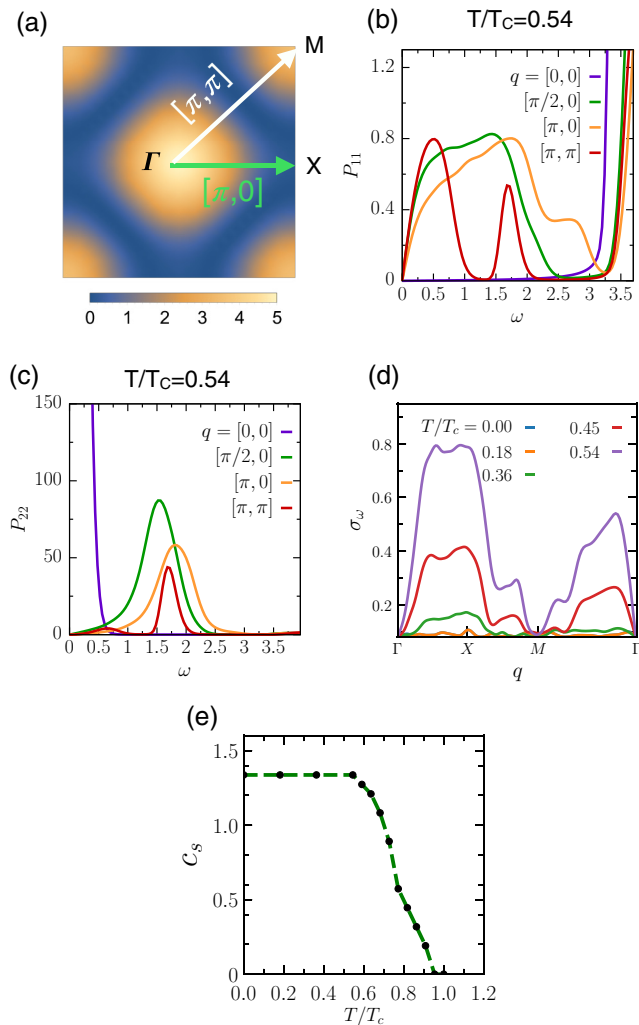


FIG. 5. (a) Color plot of the dispersion of a clean superconductor in the square lattice Brillouin zone. The wave vector $[\pi, \pi]$, shown with white arrow, connects momenta where the dispersion is almost same. This leads to a low threshold for incoherent spectral weight due to quasiparticle scattering near $[\pi, \pi]$. On the other hand, the wave vector $[\pi, 0]$ connects momenta with large difference in dispersion. Hence, the energy threshold for incoherent weight is large near $[\pi, 0]$. (b), (c) The EDC curves for (b) P_{11} and (c) P_{22} are shown for specific q values at $T = 0.54 T_c$. (d) Width of the dispersive collective modes in ω , (σ_ω , obtained from the phase sector P_{22}) as a function of q values for different temperature values of T . We notice that the collective mode remains sharp at Γ and M points, while it broadens with temperature at intermediate momenta. (e) The sound velocity is plotted as a function of T/T_c . It remains almost constant up to $T/T_c \sim 0.54$, then rapidly decreases to zero near T_c .

mode remains sharp at $q = [0, 0]$ and $[\pi, \pi]$, while the broadening at intermediate momenta increases with increasing temperature.

We note that our treatment ignores the long-range Coulomb interactions between charged electrons which are present in real materials and focuses on the effective attractive interaction that creates a superconducting state in the system. Long-range Coulomb interactions in a clean three-dimensional superconductor are known to gap out the long-wavelength

phase modes and push them to the plasma frequency via the Anderson-Higgs mechanism [47]. However, in two dimensions, the plasmon dispersion is not gapped; rather it follows a $\sim \sqrt{q}$ dispersion [48]. In a disordered system with broken translational invariance, the plasmon dispersion at long wavelengths can get modified. There are two length scales that can cut off the long-range interaction, (a) the screening length and (b) the localization length generating an effective short-range interaction [8,49]. In Appendix D, we provide detailed estimates of these two length scales for our system. We find that the two-dimensional screened interaction has a $1/r^3$ dipolar decay and the corresponding scattering length \sim lattice spacing. The localization length is estimated to be 20 lattice spacing or larger. Thus, for our calculation, the effective length scale from screening provides the long-distance cutoff which modifies the Coulomb interaction.

So far, the effect of Coulomb interactions has been studied for *clean* superconductors in Refs. [28,37] using the standard path integral formalism. The modification of this formalism to include Coulomb interactions for the disordered superconductor is nontrivial, challenging, and an open problem. The only work on combining disordered superconductivity and Coulomb interactions has been attempted in Ref. [49], where disorder has been treated on average as a *homogeneous* film and the Coulomb interactions have been treated perturbatively. We expect the inhomogeneous superconductor, with superconducting puddles in an insulating matrix and a finite single-particle gap across the transition, to respond quite differently to Coulomb interactions. However, the details of such an inhomogeneous calculation with spatially dependent screening treated *self-consistently* remain open for future investigations.

B. Pair spectral function in disordered superconductor

We now consider the key issue which we want to study in this paper: How do the collective modes evolve with temperature in a disordered superconductor? In a disordered system, momentum is not a good quantum number for a single disorder realization. For each such realization, we first construct the pair spectral function $P_{\alpha\beta}$ as a matrix in the real space coordinates r and r' . We then work with the center of mass coordinate $R = (r + r')/2$ and relative coordinate $d = (r - r')$ and average the spectral function $P(d, R, \omega)$ over several disorder realizations. The disorder averaging restores translation invariance, i.e., the averaged quantity is a function only of d and ω . Averaging over R , we get $P(d, \omega) = 1/N_s \langle \sum_R P(d, R, \omega) \rangle$ (N_s being the number of lattice sites and $\langle \rangle$ corresponds to disorder average). We then Fourier transform the spectral function in d to express it as a function of q and ω , i.e., $P(q, \omega)$. The variation of this disorder-averaged spectral function with momentum q and energy ω will be our key tool to study the behavior of finite-temperature collective modes.

We first consider the spectral function of the disordered system at $T = 0$ (worked out in Ref. [39]), so we have a reference to understand the finite temperature variations. The amplitude and phase spectral functions P_{11} and P_{22} are plotted as a function of q and ω for a weakly disordered system with $V = 0.1 t$ in Figs. 6(a) and 6(e), respectively. While the phase

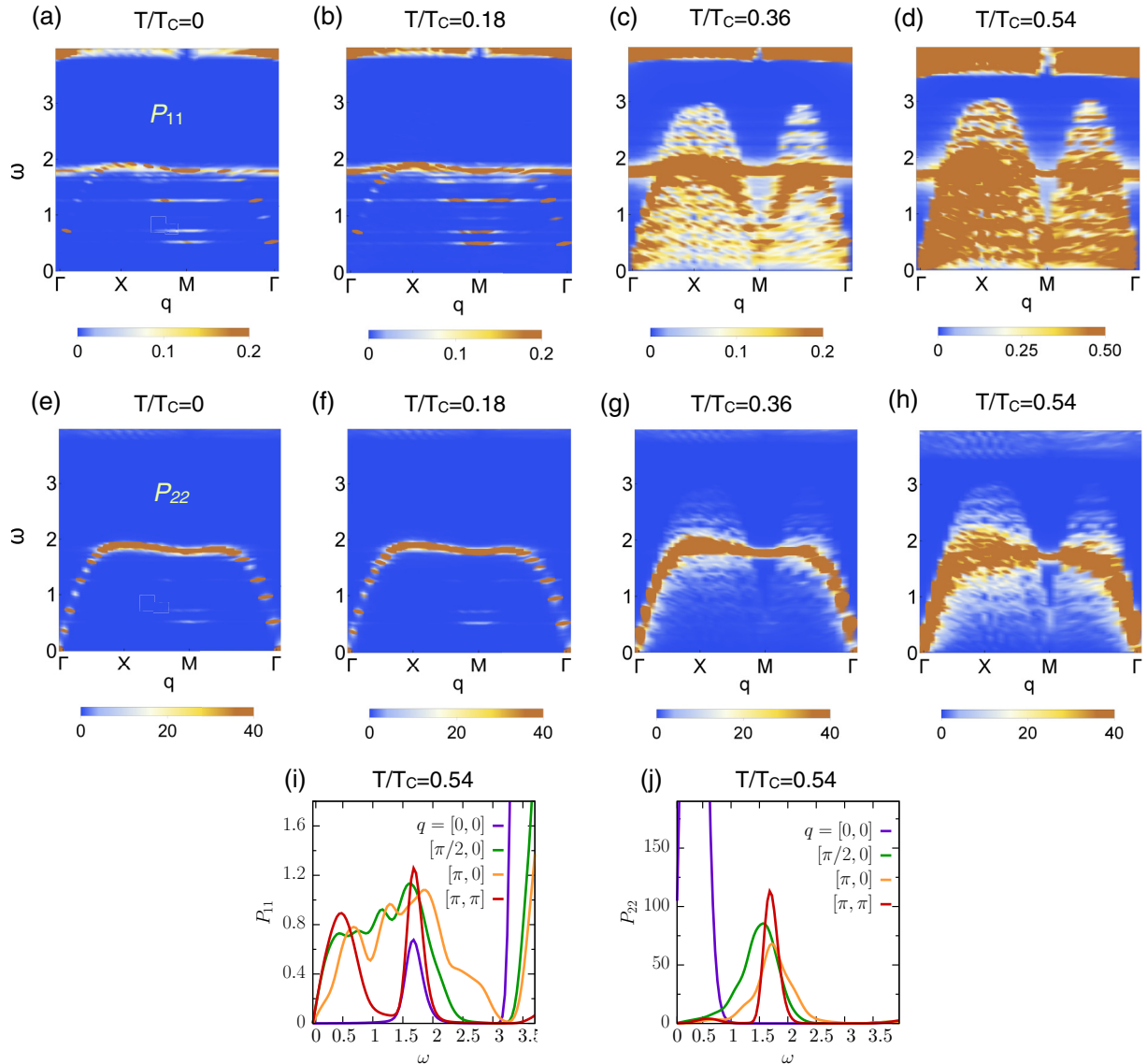


FIG. 6. Spectral functions in a weakly disordered superconductor: (a)–(d) amplitude spectral function P_{11} and (e)–(h) phase spectral function P_{22} of the pair spectral function $P(q, \omega)$ in the presence of weak disorder $V/t = 0.1$ shown as a density plot in q and ω , for increasing temperatures: $T = 0$, $T = 0.18 T_c$, $T = 0.36 T_c$, and $T = 0.54 T_c$ (corresponding to $T = 0$, $T = 0.2 t$, $T = 0.4 t$, and $T = 0.6 t$, respectively). Note the appearance of the subgap Higgs peak in the amplitude sector P_{11} at low T . While this nondispersive Higgs mode remains unaffected at momenta $\Gamma = [0, 0]$ and $M = [\pi, \pi]$ with increasing T , it gets overwhelmed by the temperature-induced background halo at other momenta. The coherent collective modes in the phase sector remain mostly unaffected at low temperatures, but they are thermally broadened at large temperatures. The EDC curves for (i) P_{11} and (j) P_{22} are shown for specific q values and for a temperature $T = 0.54 T_c$. The EDC of P_{11} clearly shows the Higgs mode at the Γ point and two distinct modes (the lower broad peak is due to the temperature-induced quasiparticle scattering, and the higher energy peak is due to disorder) at the M point. The EDC curves for P_{22} show thermally broadened dispersive collective mode peaks. All the disorder data have been obtained on a 24×24 lattice, and averaged over 15 disorder realizations.

spectral function [Fig. 6(e)] is almost unchanged from the clean case, with a linearly dispersing collective mode dominating at low energies, the amplitude spectral function shows dramatic change [Fig. 6(a)]. In contrast to the clean case, where at $q = 0$, the Higgs mode sits at the threshold of the two-particle continuum at an energy of $2\Delta_0$, a non-dispersive mode appears at an energy below two-particle continuum ($2E_{\text{gap}}$) in this case. At $q = 0$, this subgap mode is identified as the disorder-induced Higgs mode in a superconductor [39]. The $T = 0$ spectral functions for a moderately disordered

system with $V = t$ is shown in Figs. 7(a) (amplitude) and 7(e) (phase), respectively. The nondispersive mode in the amplitude spectral function gains more spectral weight and is considerably broadened, while the phase spectral function is relatively unchanged with disorder.

Next we study the effect of disorder on the amplitude and phase spectral functions at finite temperatures. Figures 6(b)–6(d) shows the amplitude spectral function $P_{11}(q, \omega)$, and Figs. 6(f)–6(h) show the phase spectral function in presence of a weak disorder $V/t = 0.1$ with increasing temperature.

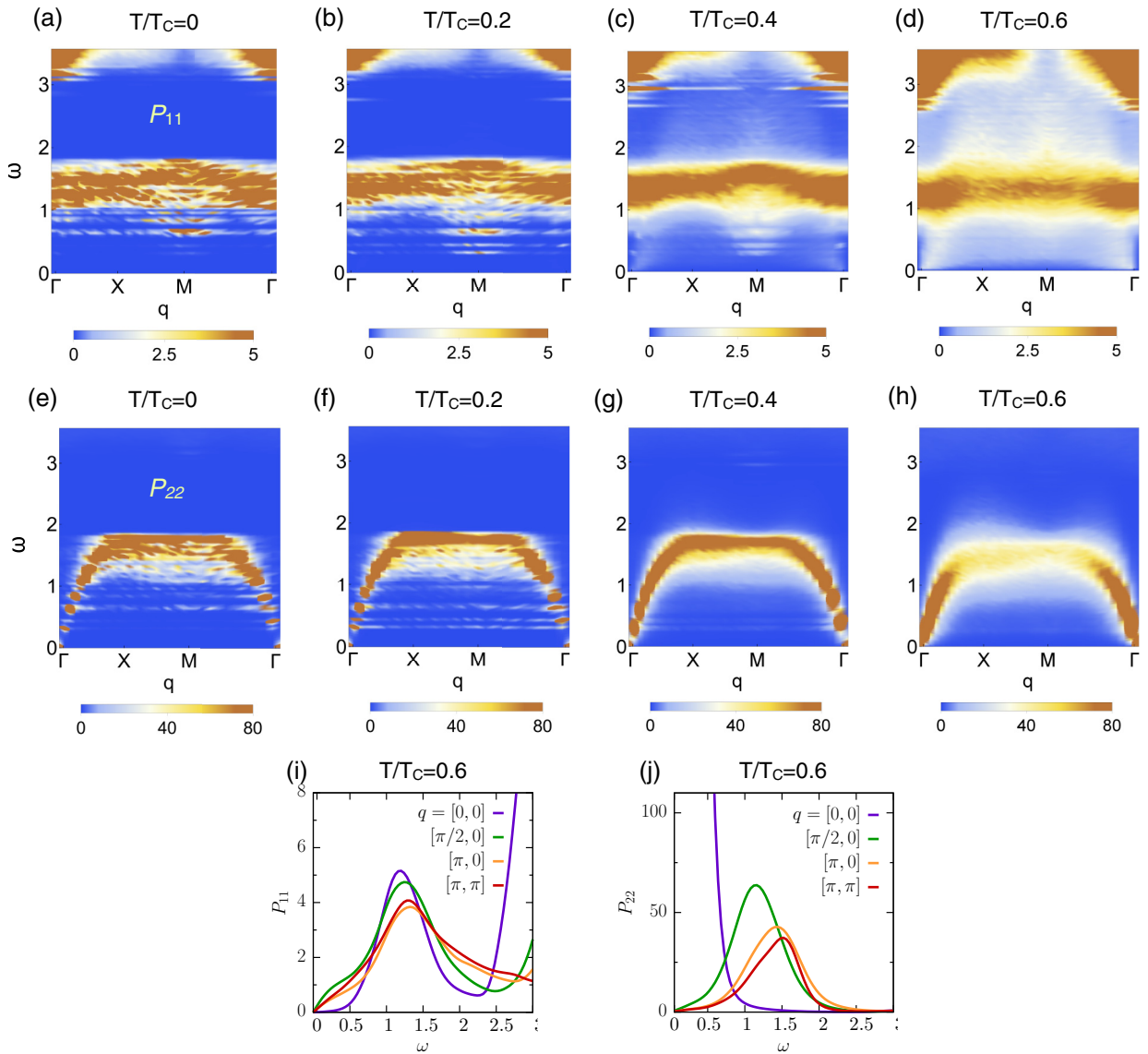


FIG. 7. Spectral functions in a moderately disordered superconductor: (a)–(d) amplitude spectral function P_{11} and (e)–(h) phase spectral function P_{22} of the pair spectral function $P(q, \omega)$ in the presence of moderate disorder $V/t = 1.0$ shown as a density plot in q and ω , for increasing temperatures: $T = 0$, $T = 0.2 T_c$, $T = 0.4 T_c$, and $T = 0.6 T_c$ (with $T_c = 1.0$). The subgap Higgs mode gets broadened and its low-energy threshold comes down in energy. With increase in temperature, contrary to the weak disorder, the lobe structure of the background halo is not seen in the amplitude sector, and the Higgs mode remains prominent at all temperatures. The EDC curves for (i) P_{11} and (j) P_{22} are shown for specific q values and for $T = 0.6 T_c$. The EDC curves for P_{11} also show that the nondispersive Higgs mode dominates at all temperatures. On the other hand, the phase sector is dominated by the dispersing collective modes, which only get thermally broadened at large temperatures.

The most visible change in the amplitude spectral functions is the appearance of the low-energy continuum weight or the halo in the background of the collective mode. As explained in the section on clean superconductors, this weight represents the scattering of the Bogoliubov quasiparticles and increases with temperature. However, for each q there is an upper bound of energy up to which the background weight exists. This background cutoff disperses linearly at small q and shows a pronounced dip around the $[\pi, \pi]$ point. Therefore the nondispersing Higgs mode near $q = 0$ and $q = [\pi, \pi]$ remains unaffected at finite temperatures [Figs. 6(b)–6(d)]. We also note that the small Higgs component in the linearly dispersing collective mode is overwhelmed by the back-

ground incoherent weight as temperature increases [Figs. 6(c) and 6(d), corresponding to $T/T_c = 0.36$ and $T/T_c = 0.54$], so the only coherent weight in the amplitude spectral function at these finite temperatures is related to the disorder-induced Higgs mode. To see this feature clearly, we plot some EDCs of the amplitude spectral function at $T = 0.54 T_c$ in Fig. 6(i). These are line cuts of the data in Fig. 6(d) at fixed values of q . The nondispersive mode at $q = 0$ is clearly seen as a peak. At $q = [\pi, \pi]$, there are two peaks, with the lower broad peak corresponding to the incoherent quasiparticle scattering and the sharper higher energy peak (at energies similar to the $q = 0$ peak) corresponding to the nondispersive Higgs mode.

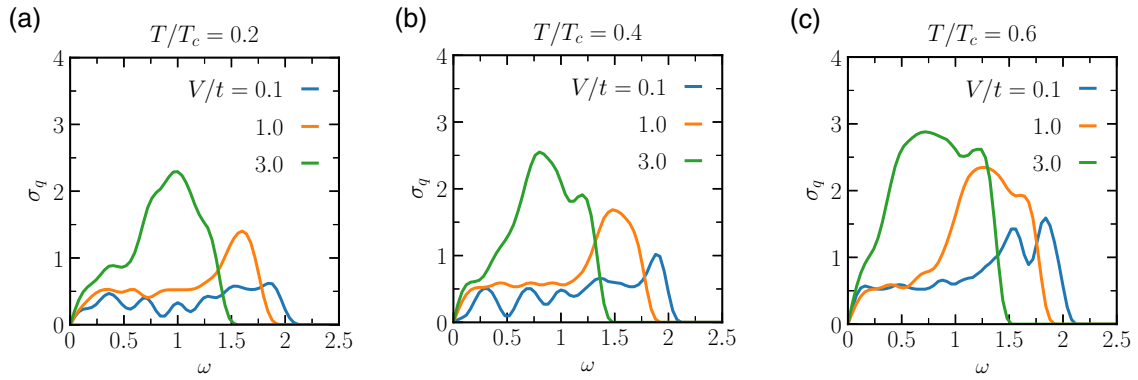


FIG. 8. (a)–(c) Width of the collective modes in q , (σ_q , obtained from the phase spectral function P_{22}) as a function of ω below two particle continuum, for (a) $T = 0.2 T_c$, $T = 0.4 T_c$, and $T = 0.6 T_c$, respectively. We note that for a fixed T , σ_q increases with increase in disorder. At small disorder, the width does not change much with energy, while the larger disorder shows a broad peak. Since with increasing disorder the collective mode structure comes down to lower energy (Figs. 6 and 7), the threshold ω at which σ_q vanishes also decreases with disorder.

On the other hand, the phase spectral function P_{22} remains mostly unaffected in the presence of weak disorder even at finite temperatures, as seen in Figs. 6(f)–6(h). While the collective mode is thermally broadened, it still dominates the low-energy phase spectral function. It is interesting to note that the mode near $[\pi, \pi]$ remains sharp at finite temperatures as the incoherent spectral weight lies below the energy of this mode. As temperature is increased [Figs. 6(g) and 6(h)], the background halo with the two-lobe structure becomes more prominent even in the phase spectral function. The variation of the phase spectral function with energy at fixed momenta at $T = 0.6 T_c$ is plotted in Fig. 6(j). The curves show thermally broadened dispersive peaks of the collective modes.

We now increase the disorder to a moderate value of $V = t$ and study the spectral functions with increasing temperature. With increase in disorder, the nondispersive Higgs mode gets broadened and its lower end comes down toward the zero energy. This mode also gains much more spectral weight. This is seen in Fig. 7(a) where we plot the spectral function at $T = 0$. As temperature is increased [Figs. 7(b)–7(d)], we once again see a diffuse background halo, but at this moderate disorder, the sharp lobe structure of the halo, which was present in the clean and the weakly disordered system, is absent. Since the sharp boundaries resulted from simultaneous momentum and energy conservation in quasiparticle scattering, and momentum conservation is strongly broken in each disorder realization at these moderate disorders, the background halo is more diffuse in this case. However, as in the weakly disordered case, the nondispersive Higgs mode remains prominent at all finite temperatures. This is clearly seen in Fig. 7(i), where we plot the variation of the amplitude spectral function with energy at fixed momenta. The curves at all the momenta show a broad peak at roughly the same energy corresponding to the nondispersive Higgs mode in the system. We note that at this moderate disorder, the edge of the continuum perceptibly comes down with increasing temperature, showing the softening of the gap in the system.

In contrast, the phase spectral function is dominated by the linearly dispersing collective mode, which is robust to both the presence of disorder and temperature [Figs. 7(e)–7(h)]. At the

largest temperature of $T = 0.6 T_c$, the collective mode near the $[\pi, 0]$ or $[\pi, \pi]$ point is broadened, but a distinct peak can still be observed, as seen in the EDCs plotted in Fig. 7(j).

We have already seen that the phase spectral function consists of a dominant dispersing collective mode. However, in a disordered system, momentum is not a good quantum number, and one would expect the collective modes to be broadened in momentum space due to elastic scattering from the impurities. To estimate the effect of this scattering, we consider the half width of the spectral function peak in the phase channel at different fixed values of ω from the momentum distribution curves. We only take into account the collective mode line between Γ and X points where the mode is dispersing, and limit our study to energies well below two particle continuum. In Figs. 8(a)–8(c), we plot this width σ_q as a function of ω for three different temperatures, $T = 0.2 T_c$, $T = 0.4 T_c$, and $T = 0.6 T_c$, respectively. Each plot contains the width for three different disorder values, a weak disorder of $V = 0.1 t$, a moderate disorder of $V = t$, and a strong disorder of $V = 3 t$, respectively. As expected, we observe that for any fixed T , σ_q increases with increasing disorder. While the low disorder width does not change much with the energy of the collective modes, the width at moderate and high disorders shows a broad peak as a function of the collective mode frequency. We also find that σ_q vanishes at a threshold ω which decreases with disorder. This happens because the whole collective mode structure itself comes down when we increase disorder (see Figs. 6 and 7).

We have already seen that the nondispersive mode in the amplitude channel produces a finite subgap spectral weight at $q = 0$, while the linearly dispersing collective mode has large weight at zero energy in the phase channel (the Goldstone mode). The phase peak and the amplitude peak are spectrally separated at $T = 0$, and hence this mode should be spectroscopically observable. We now consider whether a finite temperature will erase this spectral separation and render this mode invisible. We have plotted the amplitude and phase contribution to the spectral function for a weak disorder of $V/t = 0.1$ [Fig. 9(a)] and a moderate disorder of $V = t$ [Fig. 9(b)]. In both cases, we find that as temperature is increased, the peak positions remain unchanged while the

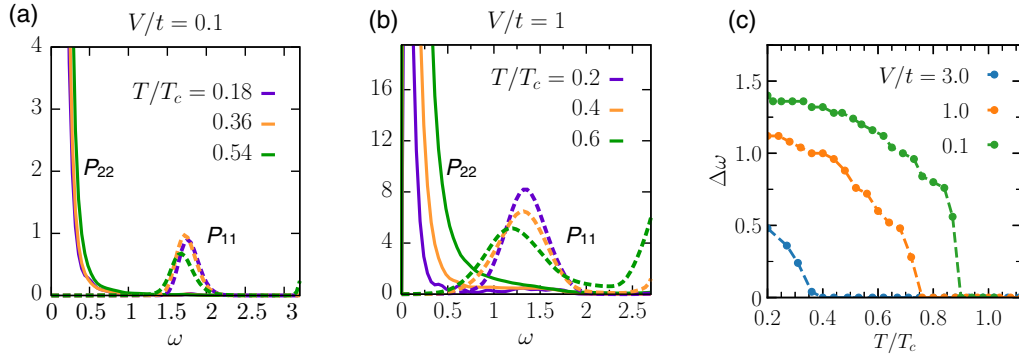


FIG. 9. (a), (b) Amplitude (P_{11} , shown as dotted lines) and phase contribution (P_{22} , shown as solid lines) to the pair spectral function P at $q = [0, 0]$ shown for two different disorder values, $V = 0.1 t$ and $V = t$, as a function of ω , and for increasing temperatures. (c) The separation between the Higgs and the phase peak, $\Delta\omega$, plotted as a function of T . We notice that at small disorders, they are separated for a large range of temperatures, while it falls rapidly to zero at a critical temperature T_c^s with increase in disorder.

broadening increases, but the separate phase and amplitude features are observable up to a reasonably high temperature. Thus, this feature is also robust to turning on temperature in the system. We note that inclusion of density fluctuations can alter the spectral separation of these features [50].

To systematically track the separation between the subgap Higgs peak and the low-energy phase peak, we define a parameter $\Delta\omega$ which indicates the separation between them in energy. In Fig. 9(c), we plot $\Delta\omega$ as a function of temperature for disorder $V/t = 0.1, 1$, and 3 . Here we extend our analysis up to large temperature values, keeping in mind that the BdG theory does not work well close to T_c . We notice that at small temperature, the Higgs and the phase modes are separated for moderately large values of disorder. However, with increase in temperature, the separation decreases monotonically and vanishes at a critical temperature T_c^s . T_c^s decreases with increase in disorder, which suggests that the sharp feature of the Higgs mode is more robust in the presence of temperature at small disorder and the robustness goes away with an increase in disorder. The momentum- and energy-resolved MEELS spectroscopy [51] should observe this Higgs mode separately from the phase pileup in an energy-resolved way.

In conclusion, in this paper we have extended our previous studies on two-particle spectral function for disordered s -wave superconductors [39] to finite temperatures. Using a functional integral formalism and Gaussian expansion around the inhomogeneous saddle point, we have studied the two-particle spectral function at small and moderately high temperatures, both in clean and disordered superconductors. We derive the analytical formulas for inverse fluctuation propagators at finite temperature, continued to real frequency. We present the full $q - \omega$ dependence of the amplitude and phase sectors of the spectral function, and therefore study the evolution of the Higgs and the Goldstone mode with temperature and disorder. We show that at finite temperatures, additional low-energy incoherent spectral weight appears in the form of lobes. In the presence of disorder, the temperature-dependent background halo competes with the collective modes in the amplitude sector. However, we find that if the disorder is not too strong, the nondispersive Higgs mode which appears as a subgap feature at $q = [0, 0]$ remains unaffected in presence of moderately high temperatures. Therefore, the Higgs mode can be seen in

an energy-resolved way separately from the low-energy phase pileup, even at experimentally accessible temperatures.

ACKNOWLEDGMENTS

A.S and R.S. acknowledge the computational facilities of the Department of Theoretical Physics, TIFR Mumbai. N.T. acknowledges support from DOE Grant No. DE-FG02-07ER46423.

APPENDIX A: SUPERFLUID STIFFNESS AT FINITE TEMPERATURE

We use Bogoliubov transformation in a disordered superconductor, which diagonalizes the effective mean-field Hamiltonian for the negative U Hubbard model, with energy E_n and the corresponding eigenfunction $[u_n(r), v_n(r)]$ [9]. Here n runs over the positive eigenvalues, i.e., $E_n > 0$. The current operator is defined as

$$j_r^x = it \sum_{\sigma} (c_{r+\hat{x}\sigma}^{\dagger} c_{r\sigma} - c_{r\sigma}^{\dagger} c_{r+\hat{x}\sigma}), \quad (\text{A1})$$

and the local kinetic energy associated with the x -directed hopping is given by

$$K_r^x = -t \sum_{\sigma} (c_{r+\hat{x}\sigma}^{\dagger} c_{r\sigma} + c_{r\sigma}^{\dagger} c_{r+\hat{x}\sigma}). \quad (\text{A2})$$

Now the superfluid stiffness by the Kubo formula is given by

$$\frac{D_s}{\pi} = \langle -K^x \rangle - \Lambda_{xx}(q_x = 0, q_y \rightarrow 0, i\omega_p = 0), \quad (\text{A3})$$

where $i\omega_p$ is the Bosonic Matsubara frequency. The first term represents the diamagnetic response to an external magnetic field which is given by

$$\begin{aligned} \langle -K^x \rangle &= \frac{4t}{N} \sum_n u_n(r + \hat{x}) u_n(r) F_n(T) \\ &+ v_n(r + \hat{x}) v_n(r) (1 - F_n(T)). \end{aligned} \quad (\text{A4})$$

The second term is the paramagnetic response given by the dynamical transverse current-current correlation function,

$$\Lambda_{xx}(\mathbf{q}, i\omega_p) = \frac{1}{N} \int_0^{1/T} d\tau e^{i\omega_p\tau} \langle j^x(\mathbf{q}, \tau), j^x(-\mathbf{q}, 0) \rangle, \quad (\text{A5})$$

which is calculated to be

$$\Lambda_{xx}(\mathbf{q}, i\omega_p) = \frac{2t^2}{N} \sum_{nm} \frac{A_{nm}(\mathbf{q})[A_{nm}(\mathbf{q}) + B_{nm}(-\mathbf{q})]}{i\omega_p + (E_n - E_m)} \times [F_n(T) - F_m(T)]. \quad (\text{A6})$$

In the above equation, n and m run over all eigenvalues (both $E_n < 0$ and $E_n > 0$), and A_{nm} and B_{nm} are given by

$$A_{nm}(\mathbf{q}) = \sum_i e^{-i\mathbf{q}\cdot\mathbf{r}} [u_n(r + \hat{x})u_m(r) - u_n(r)u_m(r + \hat{x})],$$

$$D_{nm}(\mathbf{q}) = \sum_i e^{-i\mathbf{q}\cdot\mathbf{r}} [v_n(r + \hat{x})v_m(r) - v_n(r)v_m(r + \hat{x})].$$

APPENDIX B: INVERSE FLUCTUATION PROPAGATOR FOR PHASE FLUCTUATIONS

The inverse fluctuation propagator for the phase fluctuation is given by

$$D_{22}^{-1}(r, r', \omega) = \tilde{D}_{\text{dia}}(r, r', \omega) + \omega^2 \kappa(r, r', \omega) + \Lambda(r, r', \omega).$$

The diamagnetic response \tilde{D}_{dia} is related to the local kinetic energy

$$\mathcal{K}(r, r') = -t \sum_{E_n > 0} v_n(r)v_n(r') [1 - F_n(T)] + u_n(r)u_n(r')F_n(T)$$

through the relation

$$\tilde{D}_{\text{dia}}(r, r') = -\frac{1}{2} \delta_{rr'} \sum_{\langle rr_1 \rangle} \mathcal{K}(r, r_1) + \frac{1}{2} \delta_{\langle rr' \rangle} \mathcal{K}(r, r'). \quad (\text{B1})$$

Here, the frequency-dependent compressibility κ is given by the density-density correlator,

$$\kappa(r, r', \omega) = \frac{1}{8} \sum_{E_{nn'} > 0} f_{nn'}^{(2)}(r) f_{nn'}^{(2)}(r') \chi_{nn'}(\omega) + f_{nn'}^{(1)}(r) f_{nn'}^{(1)}(r') \zeta_{nn'}(\omega), \quad (\text{B2})$$

while $\Lambda(r, r', \omega)$ is related to the paramagnetic current-current correlator on the lattice

$$\Lambda(r, r', \omega) = \sum_{\langle rr_1 \rangle \langle r'r_2 \rangle} J(r, r_1, r', r_2, \omega) - J(r, r_1, r_2, r', \omega) - J(r_1, r, r', r_2, \omega) + J(r_1, r, r_2, r', \omega), \quad (\text{B3})$$

where

$$J(r, r_1, r', r_2, \omega) = -\frac{t^2}{8} \sum_{E_{nn'} > 0} f_{nn'}^{(3)}(r, r_1) f_{nn'}^{(3)}(r_2, r') \chi_{nn'}(\omega) + f_{nn'}^{(4)}(r, r_1) f_{nn'}^{(4)}(r_2, r') \zeta_{nn'}(\omega). \quad (\text{B4})$$

The new matrix elements $f^{(3)}$ and $f^{(4)}$ are given by

$$f_{nn'}^{(3)}(r, r') = [u_n(r)v_{n'}(r') - v_n(r)u_{n'}(r')], \quad \text{and} \\ f_{nn'}^{(4)}(r, r') = [u_n(r)u_{n'}(r') + v_n(r)v_{n'}(r')]. \quad (\text{B5})$$

APPENDIX C: DAMPING OF THE HIGGS MODE ABOVE TWO-PARTICLE CONTINUUM THRESHOLD

In this Appendix, we repeat the analytic calculations [37] that show that the imaginary part of the inverse Green's function has a square root singularity. At $q = 0$, the amplitude spectral function is given by $P_{11}(0, \omega) = -\frac{1}{\pi} \text{Im} D_{11}(0, \omega) = -\frac{1}{\pi} \text{Im} \chi_{\Delta\Delta}^{-1}(0, \omega)$, where $\chi_{\Delta\Delta}$ is defined as

$$\chi_{\Delta\Delta}(q, \omega) = \frac{2}{U} + \sum_{\mathbf{k}} [u_{\mathbf{k}} u_{\mathbf{k}+\mathbf{q}} - v_{\mathbf{k}} v_{\mathbf{k}+\mathbf{q}}]^2 \times \left[\frac{1}{\omega + i0^+ - E_{\mathbf{k}} - E_{\mathbf{k}+\mathbf{q}}} - \frac{1}{\omega + i0^+ + E_{\mathbf{k}} + E_{\mathbf{k}+\mathbf{q}}} \right]. \quad (\text{C1})$$

At $\mathbf{q} = 0$, the imaginary part of $\chi_{\Delta\Delta}$ for $\omega > 2\Delta_0$ is then given by

$$\chi_{\Delta\Delta}''(0, \omega) = -\pi \sum_{\mathbf{k}} [u_{\mathbf{k}}^2 - v_{\mathbf{k}}^2]^2 \delta(\omega - 2E_{\mathbf{k}}) = -\pi \sum_{\mathbf{k}} \frac{\xi_{\mathbf{k}}^2}{E_{\mathbf{k}}^2} \delta(\omega - 2E_{\mathbf{k}}), \quad (\text{C2})$$

where $E_{\mathbf{k}} = \sqrt{\xi_{\mathbf{k}}^2 + \Delta_0^2}$. For $\omega \rightarrow 2\Delta_0 + 0^+$, the contribution to the above integral comes from momenta near the Fermi surface, or from energies near ϵ_F . In this case, one can expand $E_{\mathbf{k}} \sim \Delta_0 + \frac{1}{2} \frac{\xi_{\mathbf{k}}^2}{\Delta_0}$ and write

$$\chi_{\Delta\Delta}''(0, \omega) \sim -N(\epsilon_F) \int d\xi \frac{\xi^2}{\Delta_0^2} \delta\left(\omega - 2\Delta_0 - \frac{\xi^2}{\Delta_0}\right) \sim -N(\epsilon_F) \sqrt{\frac{\omega - 2\Delta_0}{\Delta_0}}. \quad (\text{C3})$$

We note that it is well-known that the real part of $\chi_{\Delta\Delta}(0, 2\Delta_0) = 0$ and the real part $\chi_{\Delta\Delta}' \sim \omega - 2\Delta_0$ near the two-particle continuum threshold. This shows that the Higgs propagator

$$D_{11}(0, \omega) = \frac{1}{\chi_{\Delta\Delta}(0, \omega)} \sim \frac{1}{(\omega - 2\Delta_0) + i\sqrt{\omega - 2\Delta_0}}. \quad (\text{C4})$$

Therefore, the spectral function $P_{11}(0, \omega) = -\frac{1}{\pi} \text{Im} \chi_{\Delta\Delta}^{-1}(0, \omega)$ shows an overdamped mode at $\omega = 2\Delta_0$.

APPENDIX D: ESTIMATE OF DIFFERENT LENGTH-SCALES RELEVANT TO COULOMB INTERACTION

In a purely two-dimensional system, screening of the Coulomb interaction does not lead to an exponentially decaying potential; rather it leads to a power law decay which is faster than $1/r$. If we use a Thomas-Fermi approximation for screening, the screened interaction in momentum space is given by $V_c(q) = (e^2/2\kappa\epsilon_0) \frac{1}{q+q_{\text{TF}}}$, where ϵ_0 is the permittivity of free space and κ is the dielectric constant, which is modified by the presence of substrates in two-dimensional films.

Here q_{TF} is the Thomas-Fermi wave vector. Considering the static screening of the Coulomb interaction within random phase approximation, the Thomas-Fermi wave vector is given by

$$q_{\text{TF}} = \frac{e^2}{2\kappa\epsilon_0} \rho(\epsilon_F), \quad (\text{D1})$$

where $\rho(\epsilon_F)$ is the density of states (DOS) at the Fermi energy. Now using the formula for DOS (per spin) for a square lattice with nearest-neighbor hopping near zero energy [52], $\rho(\epsilon) = \frac{1}{2\pi^2 t a^2} \ln \frac{16}{|\epsilon/t|}$, we find for a system close to half filling (considering two spins)

$$q_{\text{TF}} a = \frac{e^2}{2\pi^2 \kappa \epsilon_0 t a} \ln \frac{16}{|\mu/t|}, \quad (\text{D2})$$

where a is the lattice constant and μ is the chemical potential obtained from our calculation.

We would like to note that unlike three-dimensional systems, the Fourier transform of the Thomas-Fermi screened interaction in two dimensions does not lead to an exponentially decaying function, rather the screened potential has a form $V_c(r) \sim \frac{e^2}{4\pi\kappa\epsilon_0} \frac{1}{q_{\text{TF}}^2 r^3}$ at large r . This would, in general, be modified by the finite thickness of the film and the presence of the substrate and gates. However, even the dipolar effective interaction is short ranged, and one can define a scattering length in terms of the phase shifts of two-body wave functions [53]. For the dipolar interaction $V_{\text{dip}}(r) = d^2/r^3$, it can be shown [53] that the scattering length is $a_2 = e^{2\gamma_E} l_d$, where $\gamma_E \sim 0.577$ is the Euler constant and l_d is the dipolar length given by $l_d = md^2/\hbar^2$. Therefore, comparing with this model, we find that for screened Coulomb interaction on a

two-dimensional tight-binding model,

$$l_d = \frac{m^* d^2}{\hbar^2} = \frac{e^2}{8\pi\epsilon_0 \kappa t} \frac{1}{(q_{\text{TF}} a)^2}, \quad (\text{D3})$$

where we have used the effective mass $m^* = \hbar^2/2ta^2$. Now in our model, we have $\mu/t \approx -0.48$ (for $U/t = 5$). Therefore, for SiO_2 ($\kappa = 3.6$) and Si ($\kappa = 11.7$) substrates, we find $q_{\text{TF}} a$ to be 2.9 and 0.92, respectively, using typical lattice constant $a \sim 3 \text{ \AA}$ and hopping energy $t \sim 10 \text{ eV}$. The corresponding values of a_2/a are 0.24 and 0.77, respectively. Thus, we find that the length scales coming from screening is of the order of a lattice spacing.

On the other hand, the localization length ξ_{loc} is given by $v_F \tau$ in the weak disorder regime, where v_F is the Fermi velocity and τ is the mean-free time of the electrons in the lattice. Now, using the Fermi golden rule, it can be shown that the scattering rate is proportional to the square of the disorder potential [54], i.e., $\tau^{-1} \propto \langle V \rangle^2$, which implies that ξ_{loc} decreases with disorder. For example, for $V/t = 1$, we have $\xi_{\text{loc}} \sim \frac{1}{0.05} \frac{1}{k_F} \approx \frac{20}{k_F}$ [55]. Since we are working close to half filling, $1/k_F \sim a$. Therefore, for all our considerations, we can safely say that the screening length scale, as defined by the scattering length of the effective dipolar interaction, is much smaller than the localization length. Hence the screening length will play the role of the long-distance cutoff for the divergence of the Coulomb potential. Thus a short-range approximation is quite appropriate here. The localization length of course increases exponentially with $1/V^2$ as one goes to the weak disorder limit ($\xi_{\text{loc}} \sim e^{t^2/V^2}$). Thus, the screening length will continue to play the role of cutoff even at $V/t \sim 0.1$.

We note that the problem of determining the spatially inhomogeneous screening self-consistently, which would provide a better estimate of the length scale, remains an open problem.

-
- [1] A. M. Goldman and N. Markovic, Superconductor-insulator transitions in the two-dimensional limit, *Phys. Today* **51**(11), 39 (1998).
- [2] B. Sacépé, T. Dubouchet, C. Chapelier, M. Sanquer, M. Oviaia, D. Shahar, M. Feigel'man, and L. Ioffe, Localization of preformed Cooper pairs in disordered superconductors, *Nat. Phys.* **7**, 239 (2011).
- [3] V. F. Gantmakher and V. T. Dolgoplov, Superconductor-insulator quantum phase transition, *Phys. Usp.* **53**, 1 (2010).
- [4] Y. Dubi, Y. Meir, and Y. Avishai, Nature of the superconductor-insulator transition in disordered superconductors, *Nature (London)* **449**, 876 (2007).
- [5] G. Kopnov, O. Cohen, M. Oviaia, K. H. Lee, C. C. Wong, and D. Shahar, Little-Parks Oscillations in an Insulator, *Phys. Rev. Lett.* **109**, 167002 (2012).
- [6] N. Trivedi, R. T. Scalettar, and M. Randeria, Superconductor-insulator transition in a disordered electronic system, *Phys. Rev. B* **54**, R3756(R) (1996).
- [7] M. V. Feigel'man and M. A. Skvortsov, Universal Broadening of the Bardeen-Cooper-Schrieffer Coherence Peak of Disordered Superconducting Films, *Phys. Rev. Lett.* **109**, 147002 (2012).
- [8] I. S. Burmistrov, I. V. Gornyi, and A. D. Mirlin, Enhancement of the Critical Temperature of Superconductors by Anderson Localization, *Phys. Rev. Lett.* **108**, 017002 (2012).
- [9] A. Ghosal, M. Randeria, and N. Trivedi, Inhomogeneous pairing in highly disordered s -wave superconductors, *Phys. Rev. B* **65**, 014501 (2001).
- [10] K. Bouadim, Y. L. Loh, M. Randeria, and N. Trivedi, Single- and two-particle energy gaps across the disorder-driven superconductor-insulator transition, *Nat. Phys.* **7**, 884 (2011).
- [11] M. E. Gershenson, V. N. Gubankov, and Y. E. Zhuravlev, Interaction and localization effects in two-dimensional film of superconductor at $T > T_c$, *Solid State Commun.* **45**, 87 (1983).
- [12] M. Chand, G. Saraswat, A. Kamlapure, M. Mondal, S. Kumar, J. Jesudasan, V. Bagwe, L. Benfatto, V. Tripathi, and P. Raychaudhuri, Phase diagram of the strongly disordered s -wave superconductor NbN close to the metal-insulator transition, *Phys. Rev. B* **85**, 014508 (2012).
- [13] M. Endres, T. Fukuhara, D. Pekker, M. Cheneau, P. Schauß, C. Gross, E. Demler, S. Kuhr, and I. Bloch, The 'Higgs' amplitude mode at the two-dimensional

- superfluid/Mott insulator transition, *Nature (London)* **487**, 454 (2012).
- [14] D. Sherman, U. S. Pracht, B. Gorshunov, S. Poran, J. Jesudasan, M. Chand, P. Raychaudhuri, M. Swanson, N. Trivedi, A. Auerbach, M. Scheffler, A. Frydman, and M. Dressel, The Higgs mode in disordered superconductors close to a quantum phase transition, *Nat. Phys.* **11**, 188 (2015).
- [15] R. Matsunaga, N. Tsuji, H. Fujita, A. Sugioka, K. Makise, Y. Uzawa, H. Terai, Z. Wang, H. Aoki, and R. Shimano, Light-induced collective pseudospin precession resonating with Higgs mode in a superconductor, *Science* **345**, 1145 (2014).
- [16] R. Shimano and N. Tsuji, Higgs mode in superconductors, *Annu. Rev. Condens. Matter Phys.* **11**, 103 (2020).
- [17] D. Pekker and C. M. Varma, Amplitude/Higgs modes in condensed matter physics, *Annu. Rev. Condens. Matter Phys.* **6**, 269 (2015).
- [18] P. W. Anderson, Coherent excited states in the theory of superconductivity: Gauge invariance and the Meissner effect, *Phys. Rev.* **110**, 827 (1958).
- [19] L. Schwarz, B. Fauseweh, N. Tsuji, N. Cheng, N. Bittner, H. Krull, M. Berciu, G. S. Uhrig, A. P. Schnyder, S. Kaiser, and D. Manske, Classification and characterization of nonequilibrium Higgs modes in unconventional superconductors, *Nat. Commun.* **11**, 287 (2020).
- [20] H. Chu, M.-J. Kim, K. Katsumi, S. Kovalev, R. D. Dawson, L. Schwarz, N. Yoshikawa, G. Kim, D. Putzky, Z. Z. Li *et al.*, Phase-resolved Higgs response in superconducting cuprates, *Nat. Commun.* **11**, 1793 (2020).
- [21] L. Schwarz, B. Fauseweh, and D. Manske, Momentum-resolved analysis of condensate dynamic and Higgs oscillations in quenched superconductors with time-resolved ARPES, *Phys. Rev. B* **101**, 224510 (2020).
- [22] G. Seibold, M. Udina, C. Castellani, and L. Benfatto, Third harmonic generation from collective modes in disordered superconductors, *Phys. Rev. B* **103**, 014512 (2021).
- [23] R. Haenel, P. Froese, D. Manske, and L. Schwarz, Time-resolved optical conductivity and Higgs oscillations in two-band dirty superconductors, *Phys. Rev. B* **104**, 134504 (2021).
- [24] N. Tsuji and H. Aoki, Theory of Anderson pseudospin resonance with Higgs mode in superconductors, *Phys. Rev. B* **92**, 064508 (2015).
- [25] T. Yanagisawa, Theory of spontaneous symmetry breaking and an application to superconductivity: Nambu-Goldstone and Higgs excitation modes, *Commun. Comput. Phys.* **23**, 459 (2018).
- [26] F. Yang and M. W. Wu, Gauge-invariant microscopic kinetic theory of superconductivity: Application to the optical response of Nambu-Goldstone and Higgs modes, *Phys. Rev. B* **100**, 104513 (2019).
- [27] M. Silaev, Nonlinear electromagnetic response and Higgs-mode excitation in BCS superconductors with impurities, *Phys. Rev. B* **99**, 224511 (2019).
- [28] T. Cea, C. Castellani, and L. Benfatto, Nonlinear optical effects and third-harmonic generation in superconductors: Cooper pairs versus Higgs mode contribution, *Phys. Rev. B* **93**, 180507(R) (2016).
- [29] R. Matsunaga, Y. I. Hamada, K. Makise, Y. Uzawa, H. Terai, Z. Wang, and R. Shimano, Higgs amplitude mode in the BCS superconductors $\text{Nb}_{1-x}\text{Ti}_x\text{N}$ Induced by Terahertz Pulse Excitation, *Phys. Rev. Lett.* **111**, 057002 (2013).
- [30] R. Matsunaga, N. Tsuji, K. Makise, H. Terai, H. Aoki, and R. Shimano, Polarization-resolved terahertz third-harmonic generation in a single-crystal superconductor NbN : Dominance of the Higgs mode beyond the BCS approximation, *Phys. Rev. B* **96**, 020505(R) (2017).
- [31] G. Aad, T. Abajyan, B. Abbott, J. Abdallah, S. Abdel Khalek, A. A. Abdelalim, O. Abdinov, R. Aben, B. Abi, M. Abolins *et al.* (ATLAS Collaboration), Observation of a new particle in the search for the Standard Model Higgs boson with the ATLAS detector at the LHC, *Phys. Lett. B* **716**, 1 (2012).
- [32] S. Chatrchyan, V. Khachatryan, A. M. Sirunyan, A. Tumasyan, W. Adam, E. Aguilo, T. Bergauer, M. Dragicevic, J. Erö, C. Fabjan *et al.* (CMS Collaboration), Observation of a new boson at a mass of 125 GeV with the CMS experiment at the LHC, *Phys. Lett. B* **716**, 30 (2012).
- [33] P. B. Littlewood and C. M. Varma, Amplitude collective modes in superconductors and their coupling to charge-density waves, *Phys. Rev. B* **26**, 4883 (1982).
- [34] M.-A. Méasson, Y. Gallais, M. Cazayous, B. Clair, P. Rodiere, L. Cario, and A. Sacuto, Amplitude Higgs mode in the 2H-NbSe_2 superconductor, *Phys. Rev. B* **89**, 060503(R) (2014).
- [35] D. Podolsky, A. Auerbach, and D. P. Arovas, Visibility of the amplitude (Higgs) mode in condensed matter, *Phys. Rev. B* **84**, 174522 (2011).
- [36] S. Gazit, D. Podolsky, and A. Auerbach, Fate of the Higgs Mode Near Quantum Criticality, *Phys. Rev. Lett.* **110**, 140401 (2013).
- [37] T. Cea, C. Castellani, G. Seibold, and L. Benfatto, Non-relativistic Dynamics of the Amplitude (Higgs) Mode in Superconductors, *Phys. Rev. Lett.* **115**, 157002 (2015).
- [38] T. Cea and L. Benfatto, Nature and Raman signatures of the Higgs amplitude mode in the coexisting superconducting and charge-density-wave state, *Phys. Rev. B* **90**, 224515 (2014).
- [39] A. Samanta, A. Ratnakar, N. Trivedi, and R. Sensarma, Two-particle spectral function for disordered s-wave superconductors: Local maps and collective modes, *Phys. Rev. B* **101**, 024507 (2020).
- [40] K. A. Kouzakov and J. Berakdar, Photoinduced Emission of Cooper Pairs from Superconductors, *Phys. Rev. Lett.* **91**, 257007 (2003).
- [41] A. Trüttschler, M. Huth, C.-T. Chiang, R. Kamrla, F. O. Schumannand, J. Kirschner, and W. Widdra, Band-Resolved Double Photoemission Spectroscopy on Correlated Valence Electron Pairs in Metals, *Phys. Rev. Lett.* **118**, 136401 (2017).
- [42] C. Stahl and M. Eckstein, Noise correlations in time- and angle-resolved photoemission spectroscopy, *Phys. Rev. B* **99**, 241111(R) (2019).
- [43] S. Paeckel, B. Fauseweh, A. Osterkorn, T. Köhler, D. Manske, and S. R. Manmana, Detecting superconductivity out of equilibrium, *Phys. Rev. B* **101**, 180507(R) (2020).
- [44] S. Tarat and P. Majumdar, Tunneling spectroscopy across the superconductor-insulator thermal transition, [arXiv:1406.5423](https://arxiv.org/abs/1406.5423).
- [45] J. R. Engelbrecht, M. Randeria, and C. A. R. S. Melo, BCS to Bose crossover: Broken-symmetry state, *Phys. Rev. B* **55**, 15153 (1997).
- [46] R. B. Diener, R. Sensarma, and M. Randeria, Quantum fluctuations in the superfluid state of the BCS-BEC crossover, *Phys. Rev. A* **77**, 023626 (2008).

- [47] P. W. Anderson, Random-phase approximation in the theory of superconductivity, *Phys. Rev.* **112**, 1900 (1958).
- [48] P. W. Anderson, Plasmons, gauge invariance, and mass, *Phys. Rev.* **130**, 439 (1963).
- [49] A. M. Finkel'stein, Suppression of superconductivity in homogeneously disordered systems, *Phys. B: Condens. Matter* **197**, 636 (1994).
- [50] P. P. Poduval, A. Samanta, P. Gupta, N. Trivedi, and R. Sensarma, Subgap two-particle spectral weight in disordered s-wave superconductors: Insights from mode coupling approach, [arXiv:2201.01317](https://arxiv.org/abs/2201.01317).
- [51] A. Kogar, M. S. Rak, S. Vig, A. A. Husain, F. Flicker, Y. I. Joe, L. Venema, G. J. MacDougall, T. C. Chiang, E. Fradkin, J. V. Wezel and P. Abbamonte, Signatures of exciton condensation in a transition metal dichalcogenide, *Science* **358**, 1314 (2017).
- [52] G. Yu, Y. Yong-Hong, W. Yong-Gang, and Z. Qun, Density of states in two-dimensional square lattices around half filling with strong impurities, *Commun. Theor. Phys.* **43**, 743 (2005).
- [53] J. Hofmann and W. Zwirger, Universal relations for dipolar quantum gases, *Phys. Rev. Res.* **3**, 013088 (2021).
- [54] H. Smith and H. H. Jensen, *Transport Phenomena* (Oxford Science Publications, Clarendon Press, Oxford, 1989).
- [55] A. Datta, A. Banerjee, N. Trivedi, and A. Ghosal, New paradigm for a disordered superconductor in a magnetic field, [arXiv:2101.00220](https://arxiv.org/abs/2101.00220).